Appl. Phys. B 58, 413–420 (1994)

Applied Physics B Lasers and Optics

Stimulated Emission and Laser Action of Pr^{3+}-Doped $YAlO_3$

T. Danger, A. Bleckmann, G. Huber

Institut für Laser-Physik, Universität Hamburg, Jungiusstrasse 11, D-20355 Hamburg, Germany (Fax: +49-40/4123-6281)

Received 12 October 1993/Accepted 12 January 1994

Abstract. Groundstate absorption, fluorescence, excited-state absorption, and stimulated emission of Pr:$YAlO_3$ were measured in dependence on the polarization. The results reflect the anisotropy of the host lattice. Especially the polarized spectra of the stimulated emission fit very well with the laser data of this material. Seven cw laser transitions in the visible spectral range obtained so far in Pr:$YAlO_3$ with argon-ion laser pumping were identified in the spectra of the stimulated emission. In addition, two infrared cw laser transitions were realized. The best results were achieved for the $^3P_0 \rightarrow {}^3F_4$ laser transition at 746.9 nm with a maximum slope efficiency of 24.6%, a maximum output power of 49.6 mW, and a laser threshold of 25 mW.

PACS: 42.55.Rz

Pr^{3+} is an interesting ion for laser applications because of its large number of energy levels (Fig. 1, most data after [1]) offers many potential laser transitions. Pr:$CaWO_4$ was the first praseodymium laser realized in 1962 [2]. Since this time pulsed-laser action of this ion has been obtained in many other hosts, an overview is given by Kaminskii [3]. Recently, also cw lasers with Pr^{3+} were realized in Pr:$LaCl_3$ at low temperatures [4] and in fibres [5–8].

Pr:$YAlO_3$ is a promising laser material. It can be grown with high quality by the Czochralski technique. Furthermore, $YAlO_3$ is an oxide crystal with relatively small phonon energies because of the absence of tetrahedral sites in the lattice. Therefore, the rates of non-radiative transitions starting from the metastable $^3P_0$ and $^1D_2$ levels are expected to be small. Pulsed-laser action of Pr:$YAlO_3$ has been known since 1983 [9], but cw laser action was first published in 1993 [10, 11]. In this work the effect of the anisotropy of the host lattice on the spectroscopic behaviour of Pr:$YAlO_3$, in particular of the stimulated emission, was investigated. The spectroscopic results, which were obtained with the measurement techniques described in Sect. 1, are presented in Sect. 2. The laser data were analyzed on the basis of these spectroscopic parameters (Sect. 3). The measurement of the stimulated emission spectra verified that the laser transitions of Pr:$YAlO_3$ depend on the orientation of the crystal and confirmed the laser channels already published in [10, 11].

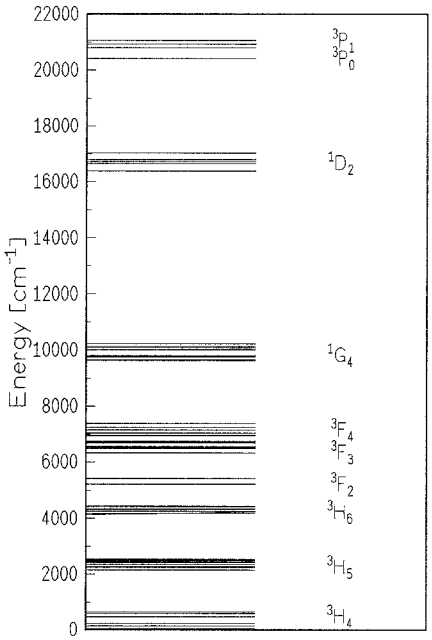

Fig. 1. Energy-level diagram of Pr^{3+} in $YAlO_3$

1 Spectroscopic Techniques

The polarized ground-state absorption spectra were measured with a spectrophotometer Cary 17 D. For the fluorescence spectra the Pr:$YAlO_3$ crystal was excited with an argon-ion laser. The polarized fluorescence was

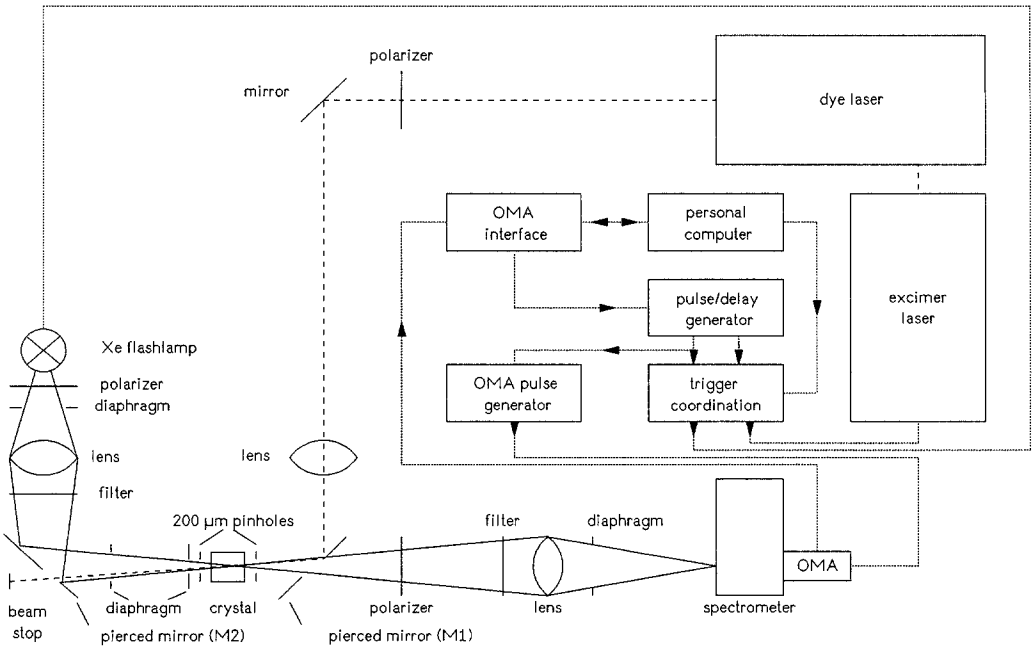

Fig. 2. Setup for the polarized and time-resolved ESA measurements

analyzed with a 0.5 m spectrometer and a S1 photomultiplier or an InSb detector. Lock-in technique led to a high signal-to-noise ratio.

The excited-state absorption and the stimulated emission spectra were measured with a pump and probe technique. The fundamental setup, except for some improvements, was described in detail by Stange [12]. Pollnau et al. [13] developed for Er^{3+}-doped $YAlO_3$ a method for eveluating time-resolved ESA measurements even on a system with a complex temporal behaviour of the population densities of the energy levels. The setup is shown in Fig. 2. The excitation of the investigated Pr(1%):$YAlO_3$ crystal was achieved by an excimer-laser pumped dye laser at a wavelength of 476.5 nm. The focussed pump beam was directed onto the crystal with a pierced Mirror (M1). The transmitted pump beam was directed through the hole of a second pierced Mirror (M2) so that the Xe flashlamp test light source was not influenced by the pump laser. The test light was directed onto the crystal via the mirror M2 with a small angle between pump and probe beam. The transmitted probe spectrum was detected with an Optical Multichannel Analyzer (OMA) behind the spectrometer. Two pinholes on both sides of the crystal secured the overlap between pump and probe beam. Time-resolved measurements were performed by adjusting a delay time Δt between pump and probe pulse.

During a measuring cycle the transmitted test spectrum with (b = both light sources triggered) and without (t = test beam) excitation, the spectrum with only the pump laser triggered (p = pump beam in order to eliminate the fluorescence of the crystal and of filters as well as scattered light of the pump laser), and the dark current of the detector (n = neither pump nor test source triggered) were recorded successively. Accumulation of hundreds or even thousands of these spectra improved the signal-to-noise ratio. According to Lambert-Beer's law, the transmitted intensities I_u in the unpumped and I_p in the pumped case are given by

$$I_u = I_0 \exp(-\sigma_{GSA} n_0 d) \tag{1}$$

and

$$I_p = I_0 \exp\left(-\left\{\sigma_{GSA} n_g + \sum_i [(\sigma_{ESA,i} - \sigma_{SE,i}) n_i]\right\} d\right). \tag{2}$$

I_0 is the incident intensity of the test beam, σ_{GSA} is the Ground-State Absorption cross section, $\sigma_{ESA,i}$ and $\sigma_{SE,i}$ are the cross sections of the Excited-State Absorption and the Stimulated Emission starting from the different excited states indicated with i. n_0 is the doping concentration density, n_i is that of the excited state i. The whole excitation density n_e and the concentration density n_g of the ground state are given by

$$n_e = \sum_i n_i, \qquad n_g = n_0 - n_e. \tag{3}$$

Of course, all these values, except for n_0, are time-dependent. Equations (1–3) yield

$$\sum_i \left[\frac{n_i}{n_e}(\sigma_{ESA,i} - \sigma_{SE,i})\right] = \sigma_{GSA} + \frac{1}{n_e d} \ln \frac{I_u}{I_p}. \tag{4}$$

The ESA measurement leads to the term

$$\ln \frac{I_u}{I_p} = \ln \frac{t-n}{b-p}. \tag{5}$$

The total excitation density n_e can be determined from the bleaching of the ground-state absorption in the spec-

trum of ln (I_u/I_p) using (4) if it is sure that no other effects like excited-state absorption or stimulated emission occur in these spectral regions. In this case the left-hand side of (4) is equal to zero, and the excitation density is given by

$$n_e = -\frac{1}{\sigma_{GSA} d} \ln \frac{I_u}{I_p}. \tag{6}$$

Using this excitation density, (4) yields the difference of the cross sections of excited-state absorption and stimulated emission for the whole spectral range, corrected for the relative excitation density n_i/n_e and summed over all possible transitions at the considered wavelength.

2 Spectroscopic Results

In Figs. 3 and 4 the polarized absorption and fluorescence spectra of Pr: $YAlO_3$ are shown. The anisotropy of the $YAlO_3$ crystal leads to different absorption coefficients and relative fluorescence intensities for the three different crystallographic directions (notation after Geller and Wood [14]). The ground-state absorption cross sections at 476.5 nm, the most effective pump wavelength when using an argon-ion laser as pump source, are $\sigma_a = 2.0 \times 10^{-20}$ cm^2, $\sigma_b = 7.9 \times 10^{-21}$ cm^2, and $\sigma_c = 2.4 \times 10^{-20}$ cm^2. The indices indicate the direction of the polarization. The anisotropy of the host lattice is also reflected by the infrared absorption and fluorescence (Figs. 5, 6).

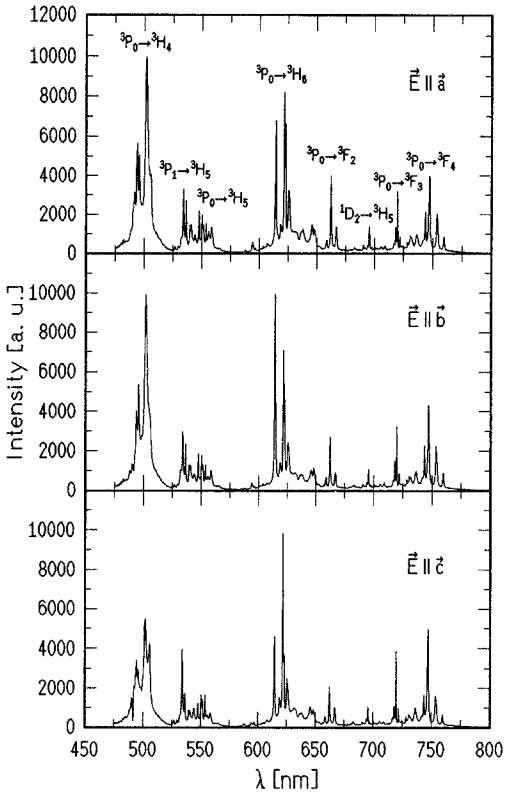

Fig. 4. Polarized fluorescence of Pr: $YAlO_3$ in the visible spectral range

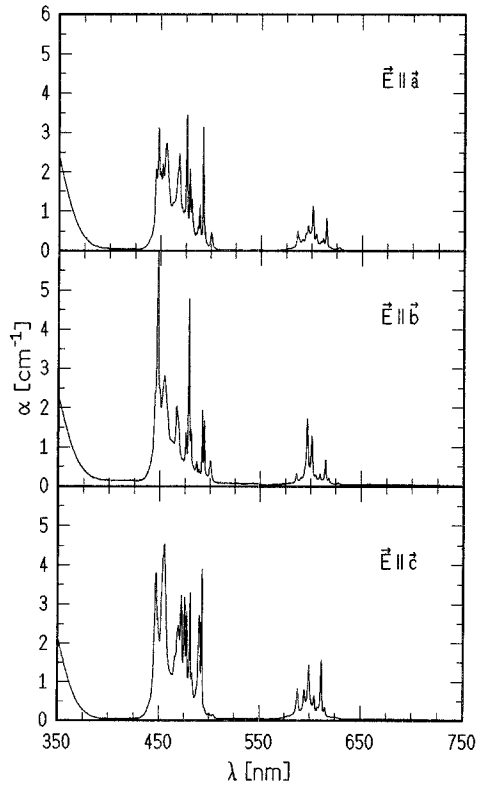

Fig. 3. Polarized absorption of Pr: $YAlO_3$

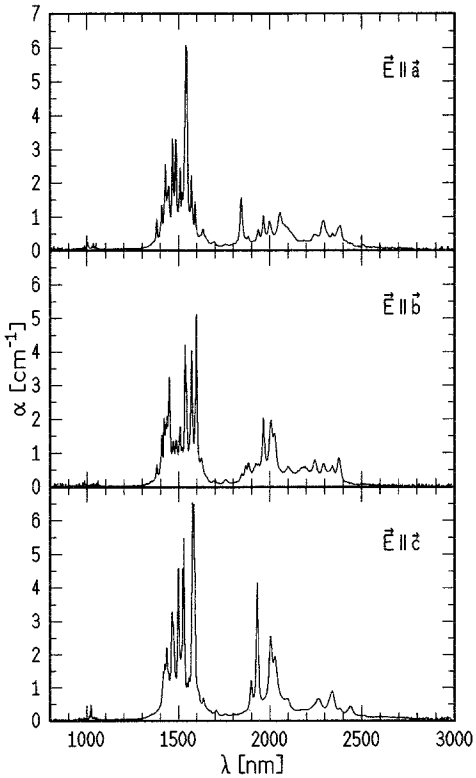

Fig. 5. Absorption of Pr: $YAlO_3$ in the infrared spectral range

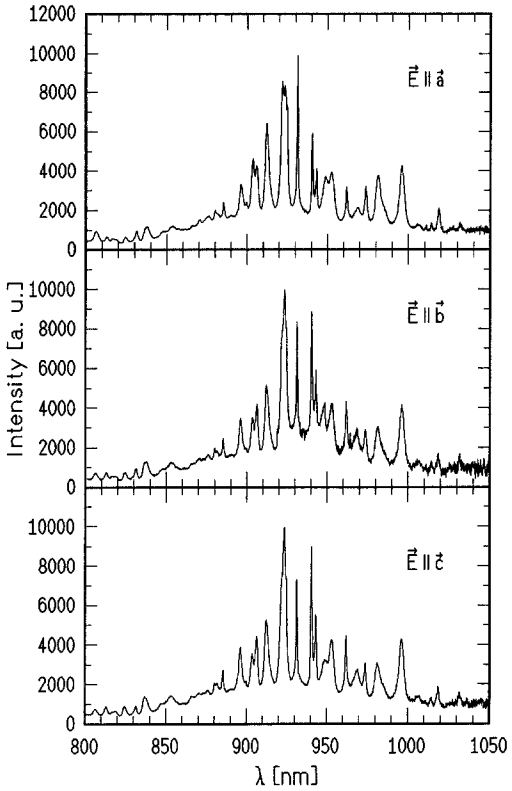

Fig. 6. Fluorescence of Pr: $YAlO_3$ in the near infrared spectral range due to several transitions

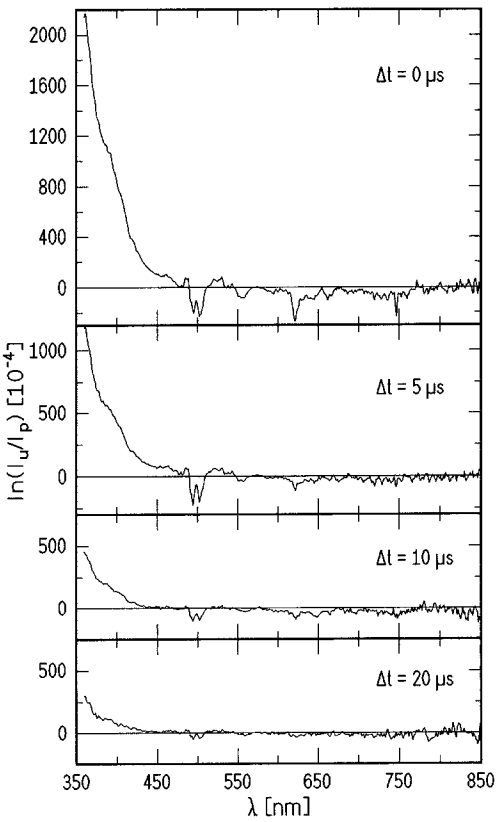

Fig. 7. Temporal behaviour of the excited-state absorption and the stimulated emission of Pr: $YAlO_3$

Table 1. Continuous-wave laser transitions of Pr: $YAlO_3$ in the visible spectral range and cross sections (in parentheses) obtained from excited-state absorption and stimulated-emission spectra. The cross sections for the stimulated emission given in parantheses were not corrected for the relative population densities

Transition	λ[nm], $(n_i/n_e)\sigma_{SE}$ [10^{-19} cm^2]		
	E∥a	**E∥b**	**E∥c**
$^3P_0 \rightarrow {}^3H_6$		613.9 (6.4)	
$^3P_0 \rightarrow {}^3H_6$	621.6 (2.6)		621.6 (5.1)
$^3P_0 \rightarrow {}^3F_2$	662.4 (1.5)		
$^3P_0 \rightarrow {}^3F_3$	719.5 (1.2)		719.5 (3.4)
$^3P_0 \rightarrow {}^3F_4$		743.7 (3.6)	
$^3P_0 \rightarrow {}^3F_4$			746.9 (7.7)
$^3P_0 \rightarrow {}^3F_4$		753.7 (3.4)	

All realized cw laser transitions [10, 11] summarized in Table 1 can easily be found in the fluorescence spectra. It is obvious that the orientation of the Pr: $YAlO_3$ crystal has a strong influence on the laser characteristics of this material, so the cw laser transitions could only be realized for special polarizations. Therefore, polarized measurements of the excited-state absorption and stimulated-emission spectra, which also allow the determination of the stimulated-emission cross sections, were performed.

The temporal behaviour of the ln (I_u/I_p) spectrum in Fig. 7 indicates that all observed transitions are correlated with the population of the $^3P_0$ state and the thermally coupled levels, in particular the $^3P_1$ state. The decay time of the excited-state absorption at wavelengths below 450 nm and of the stimulated emission is in good agreement with the $^3P_0$ fluorescence lifetime of 8.8 μs for a doping level of 1% Pr in the melt with respect to the Y site ($n_{Pr} = 1.3 \times 10^{20}$ cm^{-3} in the crystal, determined by microprobe analysis).

Excited-state absorption or stimulated-emission transitions starting from the long-lived $^1D_2$ ($\tau_{intr} = 160$ μs) or lower energy levels were not observed. This is a hint that the population densities of these levels are rather small when exciting with an argon-ion laser, although the existence of the laser channel $^1D_2 \rightarrow {}^3F_3$ in the infrared at 996 nm (outside the spectral range investigated here) under argon-ion laser excitation shows that the $^1D_2$ level is indeed populated to some extent. The transition at 996 nm was identified according to Kaminskii et al. [1]. Nevertheless, in Pr: $YAlO_3$ no transtitions in the visible range starting from other excited states have to be taken into consideration, and the sum in (4) is not necessary. The relative excitation n_i/n_e is then given by the Boltzmann factor, which is 0.7 for the $^3P_0$ level, and the fact that other energy levels, in particular the $^1D_2$ state, are occupied, too. Further investigations are necessary to determine the exact excitation densities of these levels, but it is quite probable that in Pr: $YAlO_3$ the states below the $^1D_2$ level exhibit strong non-radiative decay which leads to a negligible population density of these levels.

The excited-state absorption at shorter wavelengths was not further investigated because it is outside the main

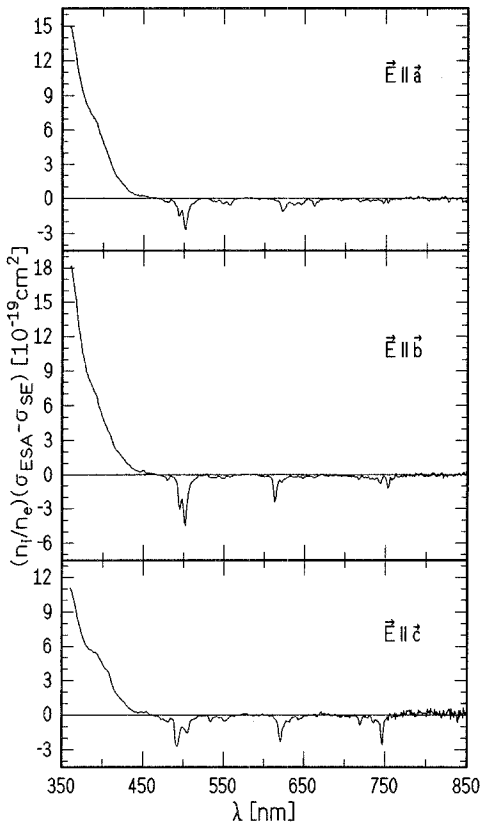

Fig. 8. Polarized excited-state absorption and stimulated emission of Pr:$YAlO_3$

pump and fluorescence regions. It is quite certain that Pr^{3+} is involved in the centre which is responsible for this absorption because it has the same decay time as the $^3P_0$ fluorescence. One possibility could be the occurence of 4f–5d or charge transfer transitions.

It is shown in Fig. 8 that the excited-state absorption and the stimulated-emission spectra of Pr:$YAlO_3$ strongly depend on the polarization. For further investigations the stimulated-emission spectra were measured with a higher resolution. The results are shown in Figs. 9–11. All cw laser transitions in this spectral range published in [10, 11] and summarized in Table 1 can be identified in these spectra. The values of the cross sections determined by the measurements of the stimulated emission were not corrected for the relative population density n_i/n_e, i.e. for the Boltzmann factor and the population of other excited states. The values of these effective cross sections are comparable to those which would be obtained from the fluorescence spectra.

A very interesting result is the stimulated emission at 533.9 nm for the polarization **E**||**c** with an effective cross section of about 1.1×10^{-19} cm^2. Although there are no reabsorption losses at this wavelength, laser action on this transition ($^3P_1 \rightarrow {}^3H_5$) could not be obtained so far. Due to the Boltzmann statistics, the population density of the upper laser level at room temperature is only 10% of the total excitation so it is more difficult to reach inversion, but the high emission cross section should allow laser oscillation. A laser test at 550 K, which only

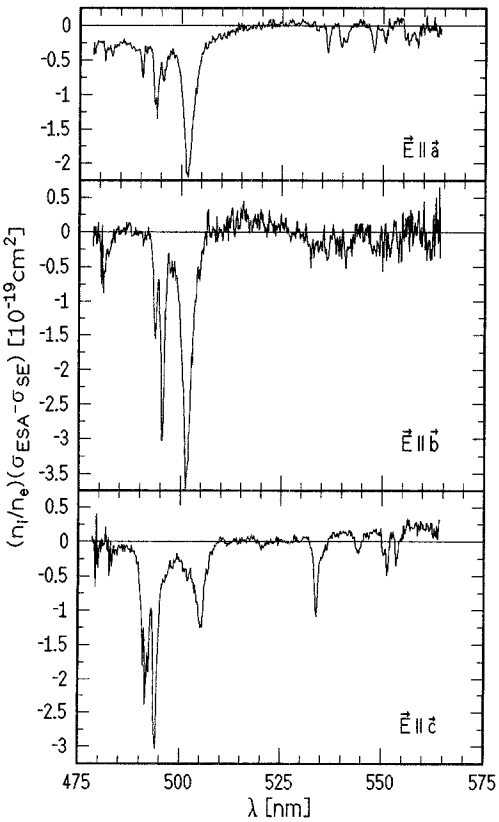

Fig. 9. Stimulated emission of Pr:$YAlO_3$

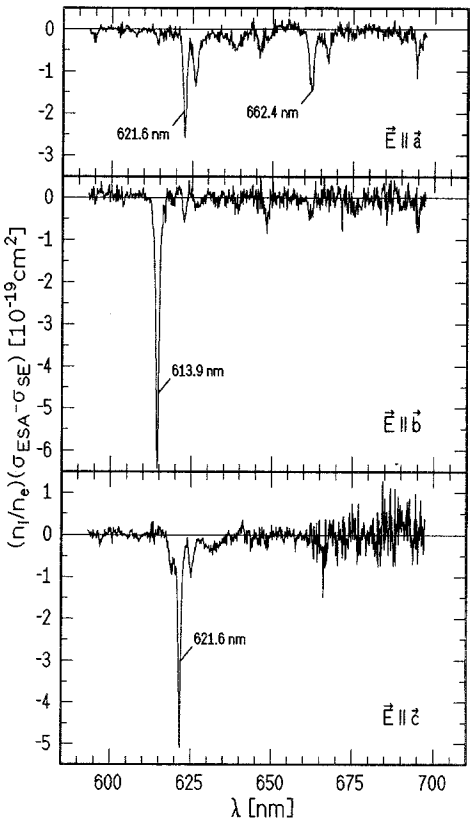

Fig. 10. Stimulated emission of Pr:$YAlO_3$. The realized cw laser transitions are indicated by their laser wavelengths

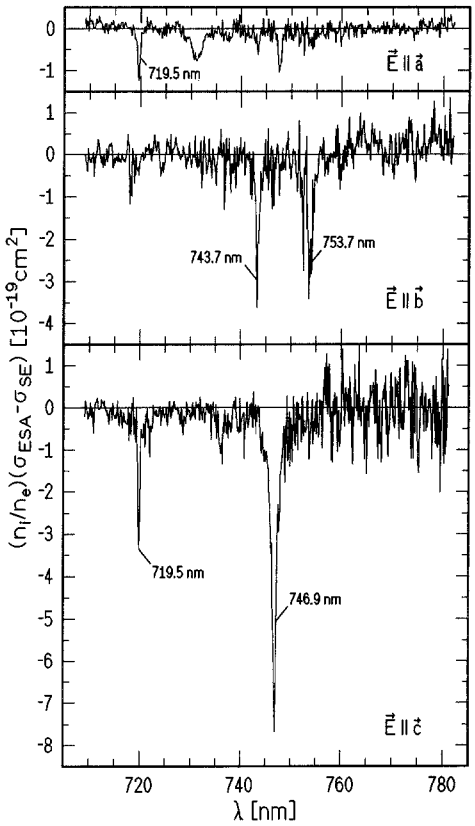

Fig. 11. Stimulated emission of Pr:$YAlO_3$. The realized cw laser transitions are indicated by their laser wavelengths

increased the Boltzmann factor to 12%, was not successful either. Further investigations of this transition and the loss processes in this spectral range are necessary in order to decide whether a green cw laser is possible in Pr:$YAlO_3$ or not.

3 Laser Experiments

For all cw laser experiments described in this work a linear, nearly concentric resonator with different dielectric mirrors of 5 cm radius of curvature was used. The Pr:$YAlO_3$ crystal was oriented along the crystallographic and indicatrix axes to avoid high birefringence losses and pumped with an argon-ion laser beam which was focussed onto the crystal with a lens of 5 cm focal length. The laser experiments were performed at room temperature. Several results have already been published [10, 11], but not yet analyzed in detail.

In order to get low pump thresholds, high slope efficiencies, and a high output power we optimized the crystal to a length of 5 mm and a Pr concentration of 8.5×10^{19} cm^{-3} (approximately 0.75% Pr in the melt with respect to the Y site). In this case reabsorption losses are kept small while the ground-state absorption is still reasonable. The excitation density n_{thr} at the laser threshold is given by

$$n_{thr}=\frac{L+T}{2\sigma_{em}d}. \tag{7}$$

L are the losses of the crystal of the length d, T is the transmission of the output coupler. σ_{em} is the emission cross section at the laser wavelength. The lowest threshold is reached by using highly reflecting mirrors ($T\approx0$). A typical value of $L=2\%$ (see below) and a cross section of 7.7×10^{-19} cm^2 of the $^3P_0\rightarrow{}^3F_4$ transition at 746.9 nm (Table 1) yield a laser threshold of $n_{thr}\approx2.6\times10^{16}$ cm^{-3} for a Pr:$YAlO_3$ crystal with a length of 5 mm. The corresponding pump power P_{thr} can be estimated by

$$P_{thr}=\frac{E_pV}{\varepsilon\tau}n_{thr}. \tag{8}$$

$E_p=hc/\lambda_p$ is the pump photon energy, V the pumped volume of the crystal, ε the pump efficiency, and τ the lifetime of the upper laser level $^3P_0$. The lifetime of the $^3P_0$ level was 9.6 μs. The pumped volume $V\approx\pi w^2d$ was estimated from a pump focus of $w\approx20$ μm. Under the assumption of $\varepsilon\approx1$ these considerations yield an expected laser threshold of about 7 mW when pumping the crystal at $\lambda_p=476.5$ nm.

The experimental results for the $^3P_0\rightarrow{}^3F_4$ laser transition at 746.9 nm are illustrated in Fig. 12. We obtained

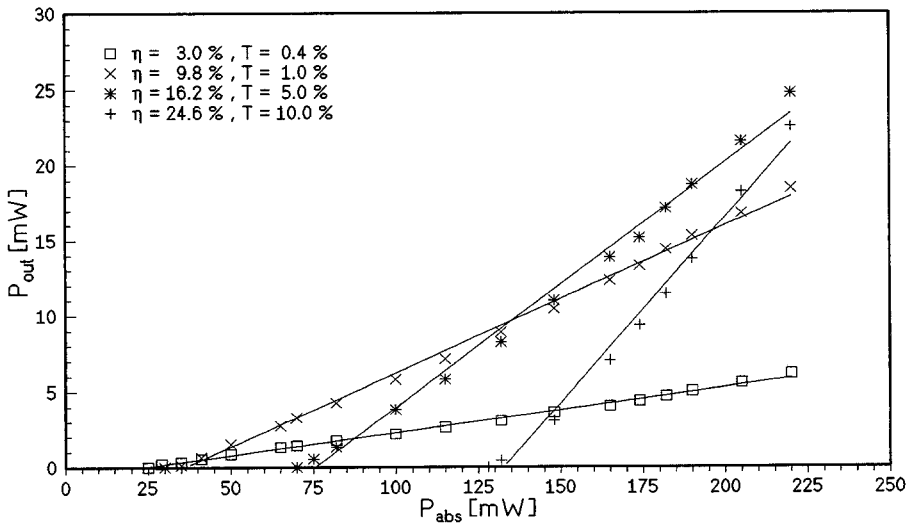

Fig. 12. Input-output diagram for the $^3P_0\rightarrow{}^3F_4$ laser transition of Pr:$YAlO_3$ at 746.9 nm when pumping at 476.5 nm

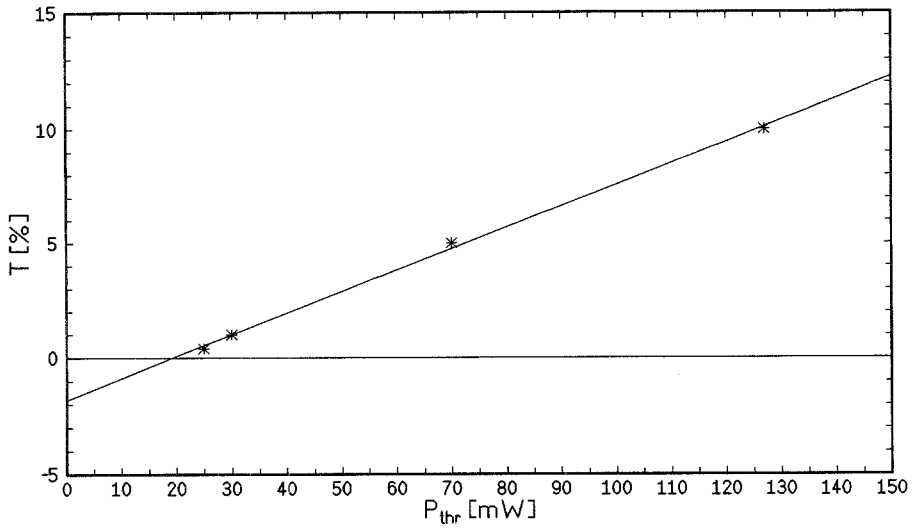

Fig. 13. Findlay-Clay plot for the $^3P_0 \rightarrow {}^3F_4$ laser transition of Pr:$YAlO_3$ at 746.9 nm when pumping at 476.5 nm

a laser threshold of $P_{thr} = 25$ mW and a slope efficiency of $\eta = 3\%$ using mirrors with a transmission of $T = 0.4\%$. The estimated theoretical values for the inversion density and the absorbed pump power at the threshold using (7) and (8) are $n_{thr} = 3.1 \times 10^{16}$ cm^{-3} (0.04% of the Pr concentration of the optimized crystal) and $P_{thr} = 8.5$ mW.

The maximum slope efficiency of 24.6% was realized with an output coupler of $T = 10\%$. In this case the pump-power threshold was increased to 130 mW. In Fig. 13 the dependence of the laser threshold P_{thr} on the transmission T is shown for the laser transition at 746.9 nm. This Findlay-Clay plot gives an estimation of the crystal losses of the order of $L \approx 2\%$. Pumping the crystal with the argon-ion laser in the multiline mode we obtained a maximum output power of $P_{out} = 49.6$ mW.

The laser data of Pr:$YAlO_3$ strongly depend on the polarization. Most of the laser transitions could be realized only in one crystallographic direction. The visible cw laser lines of Pr:$YAlO_3$ were also investigated within the measurements of excited-state absorption and stimulated emission (see Sect. 2). In addition, laser emission with **E**||**c** was realized on the $^3P_0 \rightarrow {}^1G_4$ transition at 939.5 nm and on the $^1D_2 \rightarrow {}^3F_3$ transition at 996.0 nm. All laser data are summarized in Table 2.

Table 2. Results of the cw laser experiments on Pr(0.75%):$YAlO_3$. λ_L is the laser wavelength. The results obtained with the optimized crystal are indicated with*. Different sets of mirrors were used to select special wavelengths

Transition	λ_L [nm]	Polarization	P_{thr} [mW]	P_{out} [mW]	η [%]
$^3P_0 \rightarrow {}^3H_6$	613.9	**E**||**b**	–	–	–
$^3P_0 \rightarrow {}^3H_6$	621.6	**E**||**a**, **c**	290	11.2	2.1
$^3P_0 \rightarrow {}^3F_2$	662.4	**E**||**a**	470	0.9	–
$^3P_0 \rightarrow {}^3F_3$	719.5	**E**||**a**, **c**	390	12.3	2.7*
$^3P_0 \rightarrow {}^3F_4$	743.7	**E**||**b**	410	0.7	–
$^3P_0 \rightarrow {}^3F_4$	746.9	**E**||**c**	80	27.6	5.0
$^3P_0 \rightarrow {}^3F_4$	746.9	**E**||**c**	25	49.6	24.6*
$^3P_0 \rightarrow {}^3F_4$	753.7	**E**||**b**	430	0.8	–
$^3P_0 \rightarrow {}^1G_4$	939.5	**E**||**c**	750	0.2	–*
$^1D_2 \rightarrow {}^3F_3$	996.0	**E**||**c**	830	0.1	–

The high emission cross sections of Pr:$YAlO_3$ yield another interesting effect. Three pairs of laser transitions oscillating simultaneously were observed at the following wavelengths: 662.4 nm and 719.5 nm with **E**||**a**, 743.7 nm and 753.7 nm with **E**||**b**, and 621.6 nm and 719.5 nm with **E**||**c**. All these laser transitions are competing processes because they start from the same upper laser level $^3P_0$. The effect of simultaneous multiline lasing is probably supported by spectral hole burning.

4 Conclusions

In this work it was shown that the spectroscopic properties of Pr^{3+}-doped $YAlO_3$ strongly depend on the polarization. The maximum cross sections for stimulated emission determined by these measurements are of the order of 10^{-19} cm^2. The lifetime of the $^3P_0$ level is 8.8 μs for a Pr concentration of $n_{Pr} = 1.3 \times 10^{20}$ cm^{-3}. The dependence of the stimulated emission on the polarization confirms the fact that the cw laser transitions could only be realized for special orientations of the crystal. Eight cw laser transitions starting from the $^3P_0$ level and one starting from the $^1D_2$ were realized in the red and near-infrared spectral range.

It turned out that the further investigation of the potential laser transition $^3P_1 \rightarrow {}^3H_5$ at 533.9 nm is very interesting. Although stimulated emission without internal reabsorption occurs at this wavelength for **E**||**c**, no laser action could be realized on this transition so far.

Acknowledgement. The authors wish to thank Mrs. B. Cornelisen (Mineralogisch-Petrographisches Institut, Universität Hamburg) for performing the microprobe analyses.

References

1. A.A. Kaminskii, K. Kurbanov, K.L. Ovanesyan, A.G. Petrosyan: Phys. Status Solidi (a) **105**, K 155 (1988)
2. A. Yariv, S.P.S. Porto, K. Nassau: J. Appl. Phys. **33** (8), 2519 (1962)
3. A.A. Kaminskii: *Laser Crystals. Their Physics and Properties,* 2nd edn., Springer Ser. Opt. Sci., Vol. 14 (Springer, Berlin, Heidelberg 1990)
4. M.E. Koch, A.W. Kueny, W.E. Case: Appl. Phys. Lett. **56** (12), 1083 (1990)
5. R.M. Percival, M.W. Phillips, D.C. Hanna, A.C. Tropper: IEEE J. QE- **25** (10), 2119 (1989)
6. J.Y. Allain, M. Monerie, H. Poignant: Electron. Lett. **27** (2), 189 (1991)
7. Y. Durteste, M. Monerie, J.Y. Allain, H. Poignant: Electron. Lett. **27** (8), 626 (1991)
8. R.G. Smart, J.N. Carter, A.C. Tropper, D.C. Hanna, S.T. Davey, S.F. Carter, D. Szebesta; Opt. Commun. **86**, 337 (1991)
9. A.A. Kaminskii, A.G. Petrosyan, K.L. Ovanesyan, M.I. Chertanov: Phys. Status Solidi (a) **77**, K 173 (1983)
10. A. Bleckmann, F. Heine, J.-P. Meyn, T. Danger, E. Heumann, G. Huber: Advanced Solid-State Lasers Conference, New Orleans, LA, USA, paper ATuB1 (1993)
11. A. Bleckmann, F. Heine, J.-P. Meyn, T. Danger, K. Petermann, G. Huber: In *Conference on Lasers and Electro-Optics,* OSA Technical Digest Series, Vol. 11 (Optical Society of America, Washington, DC 1993) p. 406 (paper CThF2)
12. H. Stange: Absorption aus angeregten Zuständen in Übergangsmetall-dotierten Laserkristallen. Dissertation, Universität Hamburg (1991)
13. M. Pollnau, E. Heumann, G. Huber: Appl. Phys. A **54**, 404 (1992)
14. S. Geller, E.A. Wood: Acta Crystallogr. **9**, 563 (1956)